

Pontryagin’s Principle for Leakage-Immune Adiabatic Quantum State Transfer

Xiao-Yu Dong,^{1,2} Xi-Lai Wang,^{1,2} and Wen-Long Ma^{1,2,*}

¹State Key Laboratory of Semiconductor Physics and Chip Technologies,
Institute of Semiconductors, Chinese Academy of Sciences, Beijing 100083, China

²Center of Materials Science and Opto-Electronic Technology,
University of Chinese Academy of Sciences, Beijing 100049, China
(Dated: April 14, 2026)

The standard stimulated Raman adiabatic passage (STIRAP) protocol enables high-fidelity quantum state transfer in an ideal three-level system via adiabatic following of a dark state evolution. However, in practical systems with more energy levels, control pulses with finite spectral selectivity often couple the three-level subspace to the remaining subspace, introducing leakage that fundamentally limits the transfer performance. Here, we adopt a multilevel chain model for STIRAP that explicitly incorporates this leakage subspace. Using Pontryagin’s maximum principle, we formulate a leakage-penalized quantum optimal control problem with the control pulses constrained to experimentally feasible Gaussian pulse families. We derive explicit gradients of the objective functional with respect to the pulse parameters, enabling efficient low-dimensional optimization that suppresses leakage while preserving the counterintuitive STIRAP pulse ordering. Numerical simulations for a superconducting transmon platform demonstrate that the optimized control pulses can significantly enhance the target-state transfer fidelity and provide enhanced robustness to amplitude miscalibration and detuning drifts.

I. INTRODUCTION

Scalable quantum technologies require precise control of quantum systems, typically aided by externally applied electromagnetic fields [1]. Control tasks such as quantum state transfer and quantum gates require careful design of control waveforms while respecting practical constraints on the drive amplitude and bandwidth. Quantum optimal control theory addresses this problem by optimizing a performance functional subject to the system dynamics [2, 3]. Gradient-based methods, including gradient ascent pulse engineering (GRAPE) [4, 5] and Krotov schemes [6], have proven effective in many quantum-control settings [7–11]. Related optimal-control formulations have also been developed for dissipative quantum dynamics [12]. However, practical applications require formulations that explicitly incorporate experimental drive constraints, leakage errors, and control robustness [13–16]. Recent superconducting-circuit studies further highlight the practical importance of leakage-reduction strategies in experimentally relevant control settings [17].

While GRAPE is usually formulated as a gradient-based method, it can also be viewed as a discretized implementation of the first-order optimality conditions furnished by Pontryagin’s maximum principle (PMP) [18, 19]. In particular, PMP casts the constrained optimization problem as a two-point boundary-value problem and yields first-order necessary conditions for optimality. These conditions lead directly to control-gradient expressions for numerical iteration. Recent studies have applied PMP to a range of quantum-control tasks, including time-optimal control and state generation [20–

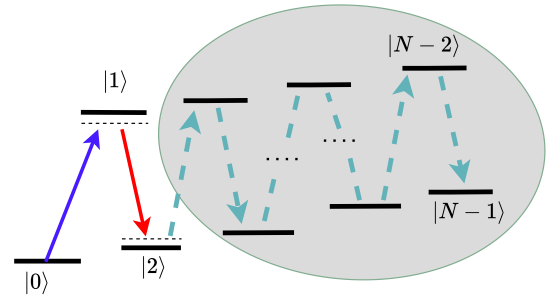


FIG. 1. Multilevel chain model for STIRAP-type population transfer with leakage. The desired transfer pathway consists of states $|0\rangle$, $|1\rangle$, and $|2\rangle$, while the shaded manifold represents higher-lying leakage states. The blue and red arrows denote the two intended couplings along the transfer pathway, and the dashed arrows indicate successive off-target couplings responsible for leakage.

[22], quantum algorithms and metrology [23, 24]. PMP-based formulations have also been extended to dissipative [25–28], stochastic [29], and open-system dynamics [30]. Compared with discrete-time gradient formulations, PMP offers a unified framework in which the system dynamics, running costs, and experimentally relevant control constraints can be incorporated on the same footing [31]. This is especially relevant for multilevel quantum control, where leakage suppression, robustness, and restricted pulse parametrizations often need to be treated simultaneously.

Stimulated Raman adiabatic passage (STIRAP) is a well-known control protocol for robust quantum state transfer, based on adiabatic following of a dark-state pathway [32–35]. In the ideal three-level model un-

* wenlongma@semi.ac.cn

der the two-photon resonance condition, STIRAP enables population transfer between the endpoint states with high fidelity while suppressing transient occupation of the intermediate state [36–38]. Its theoretical foundation is closely related to the adiabatic theorem [39]. However, realistic quantum systems seldom exhibit an exactly isolated three-level manifold. In superconducting circuits, for example, finite anharmonicity naturally leads to nearby leakage levels [40–42]. Finite-amplitude driving activates off-resonant couplings to nearby levels, and ac Stark-like shifts and limited spectral selectivity can further distort the effective dark-state structure. Dark-state transfer in multilevel settings has therefore been studied in more general chain and dark-manifold frameworks [43, 44]. Connections between optimal control and adiabatic-passage methods have also been analyzed, and optimized STIRAP-type schemes have been explored in few-level molecular settings [45, 46]. Control performance is further degraded by fluctuations, dissipation, and unwanted transitions [47–50]. In weakly anharmonic superconducting circuits, related leakage-suppression ideas have also been developed in the context of analytic pulse shaping and DRAG-type control [51, 52]. Therefore, high-fidelity STIRAP in realistic systems requires control strategies that suppress leakage and maintain robustness against parameter imperfections.

Beyond conventional adiabatic protocols, various shortcut-to-adiabaticity methods have been proposed to suppress nonadiabatic errors and accelerate state transfer [53–55]. These methods perform well in idealized few-level models, but their extension to realistic multilevel systems often introduces additional complexity [56–58]. The additional control fields used to construct the shortcut may activate unwanted transitions, and device-dependent waveform distortions and parameter-calibration errors may further degrade the performance [59, 60]. These considerations call for a unified framework that incorporates the multilevel structure, dissipative effects, and experimentally implementable pulse constraints [60, 61].

We develop a PMP-based optimal-control framework for STIRAP-type population transfer in generic multilevel systems. We first formulate the dynamics in an appropriate rotating frame and within the rotating-wave approximation (RWA) as a unified N -state nearest-neighbor chain model. This model describes the target transfer process and the dominant leakage pathways within the same effective Hamiltonian. For odd-length chains that satisfy the relevant multiphoton resonance condition, the model naturally exhibits an endpoint-connected dark-state structure. On this basis, we cast the pulse-design problem as a Bolza-type optimal-control problem with a leakage penalty, and we derive the corresponding PMP state-costate equations and control gradients in a complex Hilbert-space formulation. This formulation is fully equivalent to the standard real-variable PMP. We further restrict the control fields to a family of Gaussian pulses. This restriction reduces the origi-

nal functional optimization problem to the optimization of a small set of pulse parameters with clear physical meaning, including amplitudes, center times, and pulse widths.

We demonstrate that the above framework can be applied to anharmonic multilevel quantum systems. As a concrete example, we consider a superconducting transmon with a finite-level truncation $\{|0\rangle, \dots, |N-1\rangle\}$, and study the $|0\rangle \rightarrow |2\rangle$ transfer problem under two-tone driving while regarding the remaining states as leakage states. Within the rotating-wave approximation, we derive the corresponding effective chain Hamiltonian and detuning structure, incorporate energy relaxation into the optimization through an effective non-Hermitian description, and perform PMP-based numerical optimization over the Gaussian pulse parameters. This example is motivated both by the superconducting circuit platforms in multilevel quantum control [40–42] and recent progress on STIRAP [62, 63], superadiabatic passage [64], and related optimal-control approaches [65–67]. Related adiabatic-transfer and circuit-QED implementations have also been explored in broader superconducting settings [68–70]. Numerical results show that the optimized pulses preserve the counterintuitive temporal ordering required by STIRAP, while significantly improving the target-state transfer fidelity and enlarging the high-fidelity operating region under amplitude errors and detuning deviations. These results demonstrate that the present framework provides a practical route to STIRAP control in realistic multilevel quantum systems, with simultaneous leakage suppression and enhanced robustness.

The remainder of this paper is organized as follows. Sec. II introduces the multilevel chain model for STIRAP-type population transfer. Sec. III presents the PMP-based quantum optimal-control framework and derives the gradient formulas for parametrized Gaussian pulses. Sec. IV applies the method to a five-level transmon model and reports the numerical results for transfer performance and robustness.

II. MULTILEVEL CHAIN MODEL FOR STIRAP-TYPE POPULATION TRANSFER

An N -state nearest-neighbor chain provides a natural framework for STIRAP-type adiabatic control in multilevel systems. In a suitable interaction picture and rotating frame, the RWA removes rapidly oscillating terms and yields an effective tridiagonal Hamiltonian. The diagonal elements represent the effective detunings while the off-diagonal elements describe field-induced couplings between adjacent states in terms of effective Rabi frequencies [32–39]. In the chain basis $\{|0\rangle, \dots, |N-1\rangle\}$, the

RWA Hamiltonian takes the form

$$H(t) = \frac{\hbar}{2} \begin{bmatrix} 2\Delta_0 & \Omega_{0,1}(t) & 0 & \cdots & 0 & 0 \\ \Omega_{0,1}^*(t) & 2\Delta_1 & \Omega_{1,2}(t) & \cdots & 0 & 0 \\ 0 & \Omega_{1,2}^*(t) & 2\Delta_2 & \cdots & 0 & 0 \\ \vdots & \vdots & \vdots & \ddots & \vdots & \vdots \\ 0 & 0 & 0 & \cdots & 2\Delta_{N-2} & \Omega_{N-2,N-1}(t) \\ 0 & 0 & 0 & \cdots & \Omega_{N-2,N-1}^*(t) & 2\Delta_{N-1} \end{bmatrix}. \quad (1)$$

At this stage, no resonance condition is imposed between the endpoints of the chain. Here, $\Omega_{j,j+1}(t)$ denotes the generally complex coupling envelope for the transition $|j\rangle \leftrightarrow |j+1\rangle$, with both amplitude and phase set by the external drives. The quantities Δ_j are the effective detunings defined by the chosen rotating frame. In general, they may be nonzero for both the endpoint and intermediate states.

The multiphoton resonance conditions relevant to a given physical process enter as additional constraints. To impose an M -photon resonance between the two ends of the chain, one chooses the carrier frequencies and the rotating frame such that the effective endpoint detunings satisfy the required relation. In the simplest case, this amounts to setting the relevant diagonal mismatch to zero, or equivalently, requiring the accumulated phase mismatch between the two endpoint states to vanish. The familiar two-photon resonance condition in three-level STIRAP corresponds to the special case $M = 2$. Under such conditions, the system can adiabatically follow a dark instantaneous eigenstate.

When the drive frequencies and detunings satisfy the exact or approximate conditions required for the existence of a dark state, the chain exhibits a pronounced odd-even effect. For an odd-length chain, $N = 2n + 1$, the system can support an end-to-end dark state with zero or near-zero eigenvalue when the effective detunings on the populated even sublattice are aligned in the rotating frame. The amplitudes of this state obey a nearest-neighbor recursion relation and reside entirely on the even sublattice. This structure enables high-fidelity adiabatic transfer from $|0\rangle$ to $|N-1\rangle = |2n\rangle$ under the counterintuitive pulse sequence. Denoting the dark state by $|D_0(t)\rangle$, we write

$$|D_0(t)\rangle = \frac{1}{\mathcal{N}(t)} \sum_{k=0}^n A_k(t) |2k\rangle, \quad (2)$$

with normalization factor

$$\mathcal{N}(t) = \left(\sum_{k=0}^n |A_k(t)|^2 \right)^{1/2}, \quad (3)$$

and coefficients

$$A_k(t) = (-1)^k \prod_{m=0}^{k-1} \Omega_{2m,2m+1}^*(t) \prod_{m=k}^{n-1} \Omega_{2m+1,2m+2}(t). \quad (4)$$

Because the dark state is supported on the even sublattice, it provides an adiabatic pathway for high-fidelity

population transfer from $|0\rangle$ to $|N-1\rangle$ under the counterintuitive pulse ordering. By contrast, under the same resonance and nearest-neighbor-coupling assumptions, an even-length chain does not support the same end-to-end dark-state connectivity and therefore exhibits qualitatively different transport behavior.

More generally, in realistic multilevel systems the desired target state need not coincide with the upper end of the truncated chain. For a transfer process $|0\rangle \rightarrow |m\rangle$ with $m < N-1$, it is useful to partition the Hilbert space into a target manifold, spanned by the states directly involved in the intended transfer, and a leakage manifold containing the remaining higher-lying states:

$$\mathcal{H}_{\text{tar}} = \text{span}\{|0\rangle, |1\rangle, \dots, |m\rangle\}, \quad (5)$$

$$\mathcal{H}_{\text{leak}} = \text{span}\{|m+1\rangle, \dots, |N-1\rangle\}. \quad (6)$$

This distinction is particularly useful when the multiphoton resonance condition is imposed only on the intended transfer pathway. In that case, when the target subchain satisfies the corresponding dark-state conditions, the target manifold supports the desired STIRAP-type transport, whereas the remaining levels act as off-resonant but dynamically relevant leakage manifold induced by finite anharmonicity and unintended couplings. Even when these leakage states remain only weakly populated, they can influence the transfer through virtual excitation processes. Such processes can shift the effective detunings, renormalize the effective couplings, and distort the instantaneous dark-state structure. Realistic control models should therefore retain these states explicitly.

III. QUANTUM OPTIMAL CONTROL FRAMEWORK BASED ON PONTRYAGIN'S MAXIMUM PRINCIPLE

We employ Pontryagin's maximum principle (PMP) to iteratively update the control fields in the system Hamiltonian. PMP reformulates a constrained optimization problem as a two-point boundary-value problem involving a forward-propagated state trajectory and a backward-propagated costate trajectory [18, 19, 71]. To establish the notation used below, we first consider a general continuous-time optimal-control problem with a Bolza-type objective functional. Its objective functional is

$$J[u] = \phi(x(T)) + \int_0^T L(x(t), u(t), t) dt, \quad (7)$$

where $\phi(x(T))$ and $L(x(t), u(t), t)$ are the terminal and running costs, $x(t) \in \mathbb{R}^n$ is the system state, and $u(t) \in \mathbb{R}^m$ is the control. In quantum-control applications, the running cost may, for example, include a leakage penalty of the form $L_{\text{leak}}(\psi, t) = \langle \psi(t) | \Pi_{\text{leak}} | \psi(t) \rangle$, where Π_{leak} is the projector onto a designated leakage subspace.

Algorithm 1 PMP iterative control

Input: $u^{(0)}(t)$, x_0 , T , $\{\eta_k\}$, ε , K_{\max}
Output: Converged $u(t)$, $x(t)$, $\lambda(t)$
for $k = 0, 1, \dots, K_{\max} - 1$ **do**
 Forward propagate the state under $u^{(k)}$:
 $\dot{x}^{(k)}(t) = f^{(k)}(t)$, $x^{(k)}(0) = x_0$
 Set the terminal costate:
 $\lambda^{(k)T}(T) = -\frac{\partial\phi}{\partial x}(x^{(k)}(T))$
 Backward propagate the costate:
 $\dot{\lambda}^{(k)T}(t) = L_x^{(k)}(t) - \lambda^{(k)T}(t) f_x^{(k)}(t)$
 Evaluate the Hamiltonian:
 $\mathcal{H}_P^{(k)}(t) = \lambda^{(k)T}(t) f^{(k)}(t) - L^{(k)}(t)$
 Compute the control gradient:
 $g^{(k)}(t) = L_u^{(k)}(t) - \lambda^{(k)T}(t) f_u^{(k)}(t)$
 Update the control:
 $u^{(k+1)}(t) = u^{(k)}(t) - \eta_k g^{(k)}(t)$
if $\|u^{(k+1)} - u^{(k)}\| < \varepsilon$ **then**
 break
end if
end for
return the converged $u(t)$, $x(t)$, and $\lambda(t)$

Algorithm 1. Iterative PMP algorithm for computing the forward state trajectory, the backward costate trajectory, and the corresponding gradient-based control updates. The inputs are the initial control $u^{(0)}(t)$, the initial state x_0 , the final time T , the step-size sequence $\{\eta_k\}$, the convergence tolerance ε , and the maximum number of iterations K_{\max} .

The dynamics are constrained by

$$\dot{x}(t) = f(x(t), u(t), t), \quad t \in [0, T]. \quad (8)$$

Within PMP, the dynamical equation is treated as an infinite-dimensional equality constraint. Introducing a time-dependent Lagrange multiplier $\lambda(t) \in \mathbb{R}^n$, namely the costate, one defines the Pontryagin Hamiltonian

$$\mathcal{H}_P(x, u, \lambda, t) = \lambda^T f(x, u, t) - L(x, u, t). \quad (9)$$

The corresponding first-order necessary conditions form a two-point boundary-value problem. The state equation is

$$\dot{x}(t) = \frac{\partial \mathcal{H}_P}{\partial \lambda}(x, u, \lambda, t) = f(x, u, t), \quad (10)$$

while the costate satisfies

$$\begin{aligned} \dot{\lambda}^T(t) &= -\frac{\partial \mathcal{H}_P}{\partial x}(x, u, \lambda, t) \\ &= \frac{\partial L}{\partial x}(x, u, t) - \lambda^T(t) \frac{\partial f}{\partial x}(x, u, t), \end{aligned} \quad (11)$$

subject to the boundary conditions

$$x(0) = x_0, \quad \lambda^T(T) = -\frac{\partial \phi}{\partial x}(x(T)). \quad (12)$$

The evolution equation for $\lambda(t)$ is the adjoint equation. It propagates the influence of the terminal objective and the running cost backward in time, so in numerical implementations $\lambda(t)$ is integrated from $t = T$ to $t = 0$ using the terminal condition.

The Pontryagin Hamiltonian also determines the continuous-time functional gradient of the Bolza-type optimal-control problem with respect to the control,

$$\begin{aligned} \frac{\delta J}{\delta u(t)} &= -\frac{\partial \mathcal{H}_P}{\partial u}(x(t), u(t), \lambda(t), t) \\ &= \frac{\partial L}{\partial u}(x(t), u(t), t) - \lambda^T(t) \frac{\partial f}{\partial u}(x(t), u(t), t). \end{aligned} \quad (13)$$

This relation provides the generic gradient structure underlying PMP-based update schemes. Under the present sign convention, the control gradient is given by minus the partial derivative of the Pontryagin Hamiltonian with respect to the control.

In quantum control, the system state resides in a complex Hilbert space. Rather than decomposing the state explicitly into real and imaginary parts, we adopt a complex formulation that is fully equivalent to the real-variable PMP. For a closed quantum system governed by Schrödinger dynamics,

$$i\hbar \frac{d}{dt} |\psi(t)\rangle = H(t; u) |\psi(t)\rangle, \quad (14)$$

with a control-linear Hamiltonian

$$H(t; u) = H_0 + \sum_i u_i(t) H_i, \quad (15)$$

where $u_i(t) \in \mathbb{R}$ are real control fields, we define the real-valued Pontryagin Hamiltonian as

$$\mathcal{H}_P(\psi, \lambda, u, t) = \text{Im} \left\{ \frac{1}{\hbar} \langle \lambda(t) | H(t; u) | \psi(t) \rangle \right\} - L(\psi, u, t). \quad (16)$$

Here $\langle \lambda(t) |$ denotes the costate. The adjoint equation and terminal condition are

$$\frac{d}{dt} \langle \lambda(t) | = \frac{i}{\hbar} \langle \lambda(t) | H(t; u) - \frac{\partial L}{\partial |\psi(t)\rangle}, \quad (17)$$

$$\langle \lambda(T) | = \frac{\partial \phi}{\partial |\psi(T)\rangle}. \quad (18)$$

This construction guarantees that \mathcal{H}_P is a real scalar and is strictly equivalent to the real-variable PMP on \mathbb{R}^{2d} after decomposing the state vector into its real and imaginary parts. The continuous-time gradient with respect to each control field is then

$$\frac{\delta J}{\delta u_i(t)} = \frac{\partial L}{\partial u_i}(\psi(t), u(t), t) - \text{Im} \{ \langle \lambda(t) | H_i | \psi(t) \rangle \}. \quad (19)$$

Its discretized counterpart yields the gradient structure used in standard gradient-based quantum-control algorithms such as GRAPE [5]. Conceptually, GRAPE like-

wise combines forward state propagation with backward adjoint propagation, so the two approaches are fundamentally consistent [19].

For the N -state nearest-neighbor chain Hamiltonian introduced in the previous section, the control problem can be cast in a form naturally suited to PMP. We decompose each complex nearest-neighbor coupling as $\Omega_{j,j+1}(t) = u_j^{(x)}(t) + i u_j^{(y)}(t)$. The Hamiltonian then becomes

$$H(t) = H_d + \sum_{j=0}^{N-2} \left(u_j^{(x)}(t) X_j + u_j^{(y)}(t) Y_j \right), \quad (20)$$

where

$$H_d = \hbar \sum_{j=0}^{N-1} \Delta_j |j\rangle\langle j|, \quad (21)$$

$$X_j = \frac{\hbar}{2} \left(|j\rangle\langle j+1| + |j+1\rangle\langle j| \right), \quad (22)$$

$$Y_j = \frac{\hbar}{2} \left(i |j\rangle\langle j+1| - i |j+1\rangle\langle j| \right). \quad (23)$$

The chain model therefore has the control-linear structure required by PMP. For endpoint state-transfer problems, one may choose the target-state fidelity as the terminal objective, while the running cost may penalize intermediate-state occupation, leakage-subspace occupation, or control energy, depending on the physical objective. The optimal-control problem is then reduced to a joint optimization over the control fields $u_j^{(x)}(t)$ and $u_j^{(y)}(t)$ on each link, subject to the dynamical constraints. In this representation, PMP yields the control gradients

$$\frac{\delta J}{\delta u_j^{(x)}(t)} = \frac{\partial L}{\partial u_j^{(x)}} - \text{Im}\{\langle \lambda(t) | X_j | \psi(t) \rangle\}, \quad (24)$$

$$\frac{\delta J}{\delta u_j^{(y)}(t)} = \frac{\partial L}{\partial u_j^{(y)}} - \text{Im}\{\langle \lambda(t) | Y_j | \psi(t) \rangle\}. \quad (25)$$

The control update thus depends jointly on the forward-propagated quantum state and the backward-propagated costate, reflecting the local optimization structure of the nearest-neighbor chain model. More generally, PMP provides a unified framework for quantum optimal control: once the appropriate adjoint equation has been specified for a given dynamical model, the dynamics and the objective functional together determine the control gradient, which can then be fed back into the control parameters for iterative optimization.

This formulation is particularly natural for STIRAP-type adiabatic transfer. Within the chain model, dark-state preservation, nonadiabatic deviation, and leakage suppression can all be expressed through subspace projections and incorporated into a unified objective functional. For the multistate-chain STIRAP problem considered here, the same framework naturally accommodates closed-system evolution, effective non-Hermitian

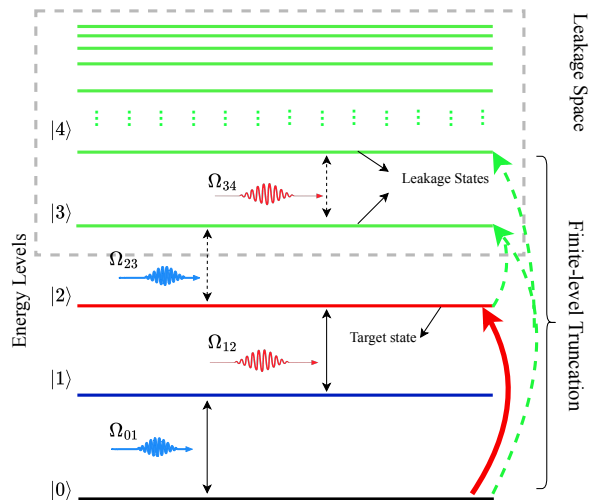


FIG. 2. Five-level truncation of a transmon ladder for leakage-suppressed STIRAP control. The target process is the population transfer $|0\rangle \rightarrow |2\rangle$, whereas $|3\rangle$ and $|4\rangle$ are treated as explicit leakage states. The adjacent couplings Ω_{01} , Ω_{12} , Ω_{23} , and Ω_{34} define the effective nearest-neighbor chain. Higher levels beyond the five-level truncation are not included explicitly.

dissipative descriptions, and more general open-system master-equation formulations. It is therefore especially well suited to multi-objective control problems involving both fidelity optimization and leakage suppression.

IV. APPLICATION TO OPTIMAL STIRAP IN A TRANSMON

We now apply the PMP-based framework developed above to leakage-suppressed STIRAP control in a weakly anharmonic superconducting transmon. Our goal is to realize the population transfer $|0\rangle \rightarrow |2\rangle$ while explicitly accounting for leakage to higher excited states induced by finite-amplitude driving. Unlike the idealized three-level STIRAP model, a realistic transmon contains nearby higher levels that cannot be fully eliminated by frequency selectivity alone [41, 42]. It is therefore necessary to embed the target transfer process in a larger multilevel manifold and optimize the pulse parameters under explicit leakage constraints [13, 14].

As a concrete example, we truncate the transmon Hilbert space to the five-level basis $\{|0\rangle, \dots, |4\rangle\}$ and treat $|3\rangle$ and $|4\rangle$ as explicit leakage states. The resulting effective chain structure is shown in Fig. 2. In this description, the target manifold is $\mathcal{H}_{\text{tar}} = \text{span}\{|0\rangle, |1\rangle, |2\rangle\}$, while $\mathcal{H}_{\text{leak}} = \text{span}\{|3\rangle, |4\rangle\}$ contains the dominant off-target process. This construction captures both the intended STIRAP transfer and the leading leakage pathways within a single RWA model [62–66].

The drift Hamiltonian is taken as

$$H_0 = \sum_{n=0}^4 E_n |n\rangle\langle n|, \quad (26)$$

where E_n are the eigenenergies of the transmon circuit. For the control term, we consider capacitive driving through the Cooper-pair number operator \hat{n} ,

$$H_c(t) = 2eV(t)\hat{n}. \quad (27)$$

To match the two-pulse structure of STIRAP, we adopt a two-tone drive,

$$V(t) = V_p(t) \cos(\omega_p t + \phi_p) + V_s(t) \cos(\omega_s t + \phi_s), \quad (28)$$

where the subscripts p and s denote the pump and Stokes components, respectively, and $V_{p/s}(t)$ are the slowly varying pulse envelopes.

Under a suitable diagonal rotating transformation and within the RWA, the driven transmon is reduced to an effective five-level nearest-neighbor chain Hamiltonian of the form

$$\tilde{H}(t) = \frac{\hbar}{2} \begin{pmatrix} 0 & \Omega_{01}(t) & 0 & 0 & 0 \\ \Omega_{01}^*(t) & 2\Delta_1 & \Omega_{12}(t) & 0 & 0 \\ 0 & \Omega_{12}^*(t) & 2\Delta_2 & \Omega_{23}(t) & 0 \\ 0 & 0 & \Omega_{23}^*(t) & 2\Delta_3 & \Omega_{34}(t) \\ 0 & 0 & 0 & \Omega_{34}^*(t) & 2\Delta_4 \end{pmatrix}, \quad (29)$$

where the effective detunings are

$$\Delta_1 = \omega_{10} - \omega_p, \quad (30)$$

$$\Delta_2 = \omega_{20} - (\omega_p + \omega_s) \equiv \delta, \quad (31)$$

$$\Delta_3 = \omega_{30} - (2\omega_p + \omega_s), \quad (32)$$

$$\Delta_4 = \omega_{40} - (2\omega_p + 2\omega_s). \quad (33)$$

Here $\omega_{jk} = (E_j - E_k)/\hbar$, and δ is the two-photon detuning associated with the target STIRAP process. Throughout this section, the nominal working point satisfies the two-photon resonance condition

$$\delta = \omega_{20} - (\omega_p + \omega_s) = 0, \quad (34)$$

while small one-photon detunings are allowed and are subsequently scanned to assess robustness.

To incorporate energy relaxation into the optimization in an efficient manner, we adopt an effective non-Hermitian description,

$$H_{\text{nh}}(t) = \tilde{H}(t) - \frac{i}{2} \sum_{\mu} C_{\mu}^{\dagger} C_{\mu}, \quad (35)$$

where the collapse operators C_{μ} represent the dominant

relaxation channels. The corresponding state equation is

$$i\hbar \frac{d}{dt} |\psi(t)\rangle = H_{\text{nh}}(t) |\psi(t)\rangle. \quad (36)$$

This effective description allows dissipation to be incorporated directly into the state propagation used in the optimization [48, 49].

The control-induced couplings are inherited from the ladder-operator matrix elements of the weakly anharmonic transmon and take the form

$$\begin{aligned} \Omega_{01}(t) &= \Omega_p(t) e^{i\phi_p}, & \Omega_{12}(t) &= \sqrt{2} \Omega_s(t) e^{i\phi_s}, \\ \Omega_{23}(t) &= \sqrt{3} \Omega_p(t) e^{i\phi_p}, & \Omega_{34}(t) &= \sqrt{4} \Omega_s(t) e^{i\phi_s}, \end{aligned} \quad (37)$$

where $\Omega_{p/s}(t) \propto 2e n_{\text{zpf}} V_{p/s}(t)$ are the effective Rabi envelopes. The same two external tones that generate the intended $|0\rangle \leftrightarrow |1\rangle$ and $|1\rangle \leftrightarrow |2\rangle$ couplings therefore also drive the higher transitions $|2\rangle \leftrightarrow |3\rangle$ and $|3\rangle \leftrightarrow |4\rangle$. This is the central mechanism by which leakage enters the multilevel STIRAP problem.

In the absence of the higher-level couplings Ω_{23} and Ω_{34} , the target three-level manifold supports the familiar instantaneous dark state

$$|D_{\text{tar}}(t)\rangle = \frac{\Omega_{12}(t)|0\rangle - \Omega_{01}(t)|2\rangle}{\sqrt{|\Omega_{01}(t)|^2 + |\Omega_{12}(t)|^2}}. \quad (38)$$

Equivalently, by introducing the mixing angle $\theta(t)$ through

$$\tan \theta(t) = \frac{|\Omega_{01}(t)|}{|\Omega_{12}(t)|}, \quad (39)$$

one may write

$$|D_{\text{tar}}(t)\rangle = \cos \theta(t) |0\rangle - e^{i\varphi(t)} \sin \theta(t) |2\rangle, \quad (40)$$

where $\varphi(t) = \arg \Omega_{01}(t) - \arg \Omega_{12}(t)$. Under the standard counterintuitive pulse ordering, $\theta(t)$ is swept smoothly from 0 to $\pi/2$, and adiabatic following of this dark state realizes the transfer $|0\rangle \rightarrow |2\rangle$ [32–34, 38]. In the full five-level transmon, however, $|D_{\text{tar}}(t)\rangle$ is no longer an exact eigenstate because the higher transitions admix leakage amplitudes and distort the dark-state pathway.

To keep the controls experimentally implementable, we restrict both drive envelopes to Gaussian pulses,

$$\Omega_{p/s}(t) = A_{p/s} \exp \left[-\frac{(t - t_{0p/s})^2}{2\sigma_{p/s}^2} \right]. \quad (41)$$

The optimization variables are then reduced to the six physically transparent pulse parameters

$$\mathbf{u} = (A_p, A_s, t_{0p}, t_{0s}, \sigma_p, \sigma_s). \quad (42)$$

Rather than optimizing arbitrary waveforms, we optimize only over this finite-dimensional parameter set. This restriction preserves the pulse smoothness and bandwidth

properties required in experiment while still allowing substantial flexibility in pulse overlap, peak amplitudes, and relative timing.

We formulate the pulse design as a Bolza-type optimal-control problem. For a state initialized in $|0\rangle$, the performance functional is chosen as

$$J(\mathbf{u}) = w_f(1 - |\langle 2|\psi(T; \mathbf{u})\rangle|^2) + \int_0^T [w_1 P_1(t) + w_{\text{leak}}(P_3(t) + P_4(t))] dt, \quad (43)$$

where $P_n(t) = |\langle n|\psi(t)\rangle|^2$ denotes the instantaneous population of level $|n\rangle$. Because H_{nh} generates non-unitary evolution, the quantities $P_n(t)$ are understood here as unnormalized state weights in the effective no-jump description. The terminal term penalizes target-state infidelity, while the running cost penalizes transient occupation of the intermediate state $|1\rangle$ and the explicit leakage states $|3\rangle$ and $|4\rangle$. This choice directly reflects the dominant error process of multilevel STIRAP in a weakly anharmonic device [47, 50]: occupation of $|1\rangle$ signals departure from the desired dark-state pathway, whereas occupation of $|3\rangle$ and $|4\rangle$ quantifies leakage induced by finite anharmonicity and off-resonant excitation.

Because the control fields are parametrized by Eq. (41), the functional gradients derived in Sec. III can be converted into parameter gradients through

$$\frac{\partial J}{\partial u_k} = \int_0^T \left[\frac{\delta J}{\delta \Omega_p(t)} \frac{\partial \Omega_p(t)}{\partial u_k} + \frac{\delta J}{\delta \Omega_s(t)} \frac{\partial \Omega_s(t)}{\partial u_k} \right] dt, \quad (44)$$

where $u_k \in \{A_p, A_s, t_{0p}, t_{0s}, \sigma_p, \sigma_s\}$. The required Gaussian derivatives are analytic:

$$\frac{\partial \Omega_\mu(t)}{\partial A_\mu} = \frac{\Omega_\mu(t)}{A_\mu}, \quad \mu \in \{p, s\}, \quad (45)$$

$$\frac{\partial \Omega_\mu(t)}{\partial t_{0\mu}} = \Omega_\mu(t) \frac{t - t_{0\mu}}{\sigma_\mu^2}, \quad \mu \in \{p, s\}, \quad (46)$$

$$\frac{\partial \Omega_\mu(t)}{\partial \sigma_\mu} = \Omega_\mu(t) \frac{(t - t_{0\mu})^2}{\sigma_\mu^3}, \quad \mu \in \{p, s\}. \quad (47)$$

The PMP iteration therefore yields a direct gradient-based optimization over a small set of pulse parameters with clear experimental interpretation [18, 19].

We initialize the optimization with a conventional counterintuitive Gaussian STIRAP pair in which the Stokes pulse precedes the pump pulse. This initial guess already gives reasonably good transfer within the target manifold, but its performance is degraded by the multilevel leakage process discussed above. The PMP update then adjusts the amplitudes, pulse centers, and widths to reduce the leakage penalty while preserving the underlying STIRAP mechanism. The numerical simulations were implemented using QuTiP and related Python-based tools [72, 73].

Fig. 3 summarizes the optimized pulse pair and the corresponding population dynamics. The optimized so-

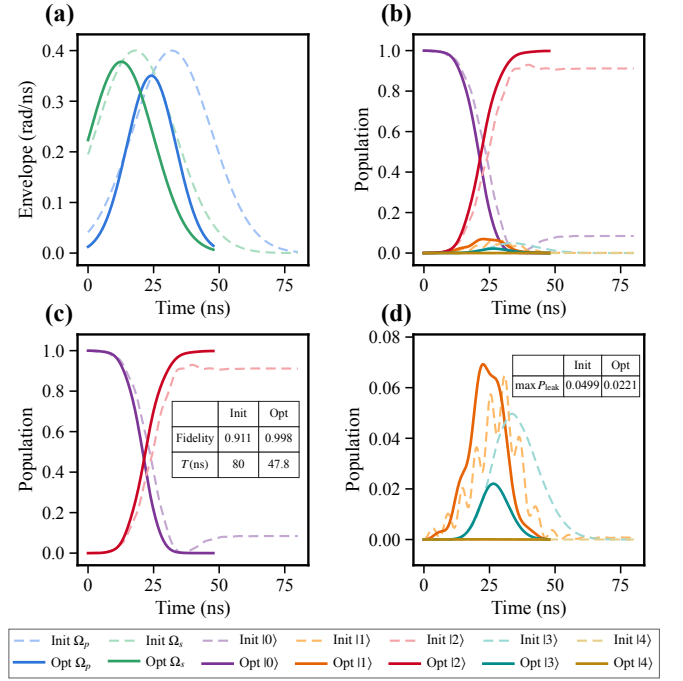


FIG. 3. Initial and PMP-optimized Gaussian protocols for the five-level transmon chain. (a) Pump and Stokes envelopes for the initial (dashed) and optimized (solid) pulses. The optimized protocol retains the counterintuitive STIRAP ordering while substantially shortening the total duration. (b),(c) Time-dependent level populations for the initial and optimized protocols, respectively. Relative to the initial protocol, the optimized pulses increase the final population of the target state $|2\rangle$ and reduce transient occupation of the penalty states $|1\rangle$, $|3\rangle$, and $|4\rangle$. (d) Leakage population for the two protocols. Insets report the transfer fidelity, total pulse duration, and maximum leakage population.

lution retains the counterintuitive pulse ordering characteristic of STIRAP, with the Stokes pulse still preceding the pump pulse. The optimization therefore preserves the underlying adiabatic-transfer mechanism rather than replacing it with a qualitatively different strategy. At the same time, the pulse widths and overlap are reshaped substantially, leading to a shorter overall protocol. According to the inset in Fig. 3(a), the total duration is reduced from 80 ns for the initial protocol to 47.8 ns for the optimized one.

Most importantly, the optimized protocol yields a substantial improvement in transfer performance. The final target-state fidelity increases from 0.911 to 0.998, while the maximum leakage population,

$$P_{\text{leak}}(t) = P_3(t) + P_4(t), \quad (48)$$

is reduced from 0.0499 to 0.0221. The population traces further show reduced transient occupation of both the intermediate state $|1\rangle$ and the leakage states $|3\rangle$ and $|4\rangle$. The optimized evolution thus remains closer to the target dark-state transfer pathway while avoiding the off-

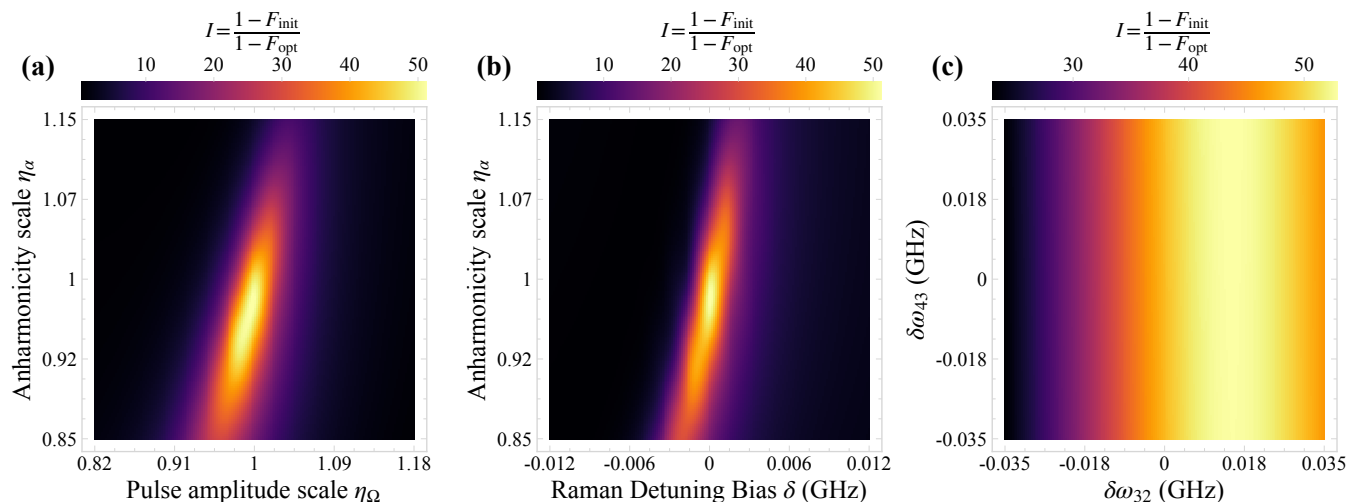


FIG. 4. Improvement landscapes for the PMP-optimized protocol relative to the initial Gaussian protocol, quantified by $I = (1 - F_{\text{init}})/(1 - F_{\text{opt}})$, over representative parameter planes. (a) Pulse-amplitude scale η_{Ω} versus anharmonicity scale η_{α} . (b) Raman-detuning bias δ versus anharmonicity scale η_{α} . (c) Higher-transition frequency offsets $\delta\omega_{32}$ and $\delta\omega_{43}$. Brighter colors correspond to larger improvement factors and hence stronger suppression of transfer error by the optimized protocol.

target manifolds opened by the weak anharmonicity of the transmon.

The simultaneous increase in fidelity and reduction in pulse duration is nontrivial. In a multilevel ladder system, a shorter protocol generally broadens the pulse spectrum and can enhance unwanted transitions. The observed improvement therefore does not arise from a naive speedup alone. Instead, the optimization identifies a more favorable balance between adiabatic following and leakage suppression by reshaping the pulse overlap and relative timing within the experimentally admissible Gaussian family.

To assess robustness more systematically, we compare the optimized protocol with the initial protocol over a range of perturbed parameters. As a compact diagnostic, we define the improvement factor

$$I = \frac{1 - F_{\text{init}}}{1 - F_{\text{opt}}}, \quad (49)$$

where F_{init} and F_{opt} denote the final target-state fidelities obtained from the initial and optimized protocols under the same perturbed condition. Values $I > 1$ indicate that the optimized protocol reduces the transfer error relative to the initial one, and larger values correspond to stronger improvement.

Fig. 4 shows the resulting improvement landscapes on several representative parameter planes. In Fig. 4(a), we scan the pulse-amplitude scale η_{Ω} together with the anharmonicity scale η_{α} . A broad bright ridge appears around the nominal operating point and extends diagonally across the parameter plane, indicating that the optimized protocol remains advantageous under correlated variations of the drive strength and the level anharmonicity. Since these two parameters jointly control

how strongly the higher transitions are activated and how severely the target dark-state pathway is distorted, the ridge structure shows that the optimization suppresses the dominant multilevel error mechanism rather than merely improving the fidelity at a single isolated point.

A similar conclusion follows from Fig. 4(b), where the Raman detuning bias δ is varied together with η_{α} . The high-improvement region forms a narrow tilted band crossing the neighborhood of the nominal working point. The optimized protocol is therefore markedly less sensitive to simultaneous variations in the two-photon resonance condition and the effective anharmonicity. Because both perturbations deform the adiabatic dark-state pathway and enhance off-resonant admixture, their joint suppression indicates that the PMP optimization targets the physically relevant source of performance degradation.

Fig. 4(c) probes the sensitivity to uncertainty in the higher transition frequencies through the offsets $\delta\omega_{32}$ and $\delta\omega_{43}$. Here the improvement factor remains high over a broad region of parameter space, with only a comparatively weak dependence on $\delta\omega_{43}$. This indicates that the optimized protocol is particularly effective in reducing the influence of the first leakage transition adjacent to the target manifold, while the next higher transition plays a smaller role over the scanned range. Such behavior is consistent with the physical intuition that, in a weakly anharmonic ladder, the dominant deformation of the target STIRAP process is set primarily by the nearest leakage levels.

To complement these two-dimensional scans, we also perform one-dimensional robustness cuts around the nominal operating point. The varied parameters are the global drive-frequency shift $\delta\omega_d$, a common transition-frequency drift $\delta\omega$, the anharmonicity scale η_{α} , the pulse-scale η_t , the Raman detuning bias δ , and the pulse-

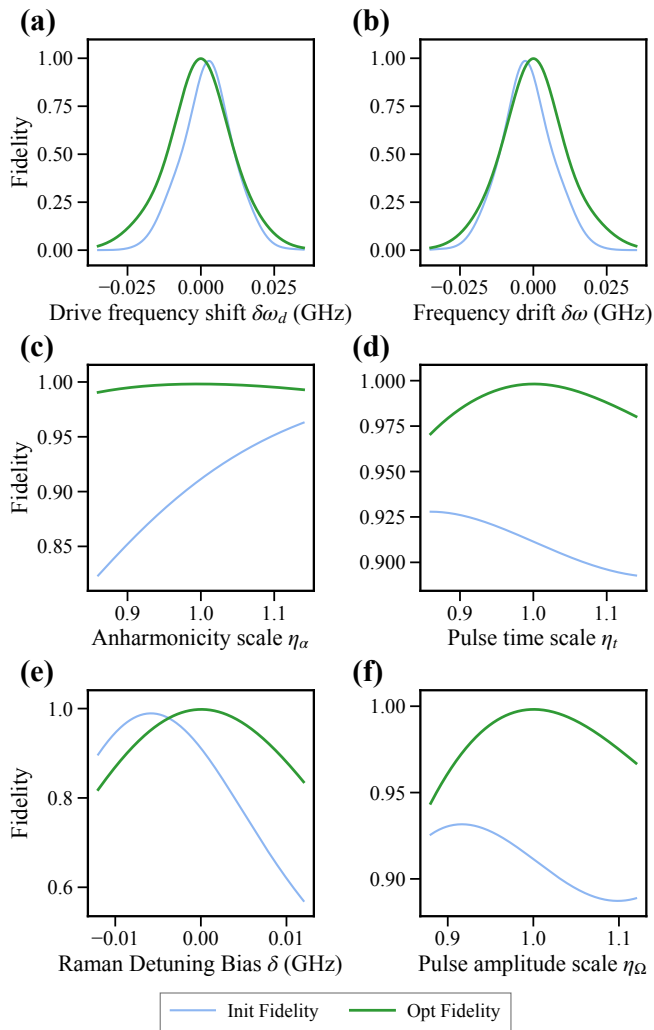


FIG. 5. One-dimensional robustness cuts for the initial and PMP-optimized protocols. The final target-state fidelity is plotted versus (a) the global drive-frequency shift $\delta\omega_d$, (b) the common transition-frequency drift $\delta\omega$, (c) the anharmonicity scale η_α , (d) the pulse-time scale η_t , (e) the Raman-detuning bias δ , and (f) the pulse-amplitude scale η_Ω . Relative to the initial protocol, the optimized protocol retains a broader high-fidelity region across all scans.

amplitude scale η_Ω . For the time scaling, the pulse centers and widths are rescaled according to

$$t_{0\mu} \rightarrow \eta_t t_{0\mu}, \quad \sigma_\mu \rightarrow \eta_t \sigma_\mu, \quad \mu \in \{p, s\}, \quad (50)$$

whereas the amplitude scaling is implemented through

$$\Omega_\mu(t) \rightarrow \eta_\Omega \Omega_\mu(t), \quad \mu \in \{p, s\}. \quad (51)$$

The corresponding fidelity curves are displayed in Fig. 5. Panels (a) and (b) show that the optimized protocol exhibits a broader high-fidelity peak against both drive-frequency offsets and transition-frequency drifts. The optimized pulse pair is therefore less sensitive to

calibration errors in the applied microwave frequencies and to slow fluctuations of the device frequencies. From an experimental perspective, such an enlarged frequency-tolerance window is particularly valuable because both error sources are common in repeated calibration cycles.

Fig. 5(c) and Fig. 5(d) show the behavior under variations in the anharmonicity scale and the pulse-time scale. In both cases, the optimized protocol significantly outperforms the initial one over the entire scanned range. In particular, the optimized fidelity remains close to unity over a wide interval of η_α , whereas the initial protocol deteriorates much more strongly as the device deviates from the nominal anharmonicity. This again supports the central physical picture: the optimized pulses are not merely tuned to a single idealized parameter set, but instead reshape the evolution so that the transfer mechanism is less vulnerable to multilevel distortions of the dark-state pathway. The improvement under pulse-time rescaling further shows that the optimized solution tolerates moderate temporal stretching and compression, which is important for implementations subject to finite timing-calibration errors or waveform distortions.

The strongest contrast appears in the Raman-detuning scan shown in Fig. 5(e). The initial protocol exhibits a marked asymmetry together with a rapid loss of fidelity once the Raman bias moves away from the nominal condition. By contrast, the optimized protocol retains a substantially broader and more symmetric high-fidelity region, indicating that the leakage-suppressed PMP optimization effectively compensates the detuning-induced deformation of the target STIRAP process. A similarly clear improvement is found in the amplitude scan of Fig. 5(f), where the optimized solution is significantly less sensitive to amplitude miscalibration. Taken together, these results show that the present optimization improves not only the nominal transfer fidelity but also the robustness margins most relevant to experiment.

Overall, the numerical results demonstrate that the present PMP-based framework provides a practical route to high-fidelity STIRAP control in realistic weakly anharmonic superconducting circuits. The optimized Gaussian pulses preserve the essential counterintuitive structure of STIRAP while substantially increasing the final transfer fidelity, shortening the total protocol duration, suppressing transient occupation of both intermediate and leakage states, and enlarging the high-fidelity operating region under parameter uncertainty. More broadly, these results show that embedding STIRAP in a constrained multilevel optimal-control framework can retain the robustness advantages of adiabatic passage while mitigating its principal limitations in experimentally relevant multilevel devices.

V. CONCLUSIONS AND OUTLOOK

In this work, we developed a PMP-based optimal-control framework for STIRAP-type population transfer

in multilevel quantum systems. By embedding the target process in an N -state nearest-neighbor chain, the method incorporates both the intended transfer process and the dominant leakage pathways within a unified effective description. It thereby captures how off-target couplings, finite anharmonicity, and dissipation degrade dark-state transfer in realistic multilevel settings.

Within this formulation, pulse design is cast as a leakage-penalized Bolza-type optimal-control problem. The corresponding state-costate equations and control gradients were derived in a complex Hilbert-space representation fully equivalent to the standard real-variable PMP. Restricting the controls to parametrized Gaussian pump and Stokes pulses reduces the original functional optimization problem to a low-dimensional search over experimentally meaningful pulse parameters, while retaining the ability to optimize fidelity, leakage suppression, and robustness within a single framework.

As a concrete application, we studied the $|0\rangle \rightarrow |2\rangle$ transfer problem in a five-level superconducting transmon model with relaxation incorporated through an effective non-Hermitian description. The optimized pulses preserve the counterintuitive ordering characteristic of STIRAP while substantially improving the transfer fidelity, suppressing transient occupation of intermediate and leakage states, and enlarging the high-fidelity operating region under amplitude miscalibration and detuning deviations. These results establish the present framework as a practical route to leakage-suppressed and robustness-enhanced STIRAP control in weakly anharmonic multilevel superconducting circuits.

Several natural extensions remain. These include full open-system formulations based on Lindblad master equations [12, 28–30], more flexible pulse parametrizations subject to experimental constraints [4–6], and robustness criteria incorporated directly into the optimal-control functional [1–3]. Such extensions would further broaden the applicability of the present framework

while preserving its central advantage: the simultaneous treatment of fidelity optimization, leakage suppression, and experimentally relevant control restrictions. More broadly, these directions may also benefit from combinations with data-driven, model-free, and reinforcement-learning-based quantum-control strategies [74, 75].

Because the present approach is built on a generic multilevel chain model together with a general PMP-based control framework, it is expected to apply broadly to other state-transfer settings in which adiabatic passage, dark-state transport, and leakage suppression must be treated simultaneously. Representative directions include STIRAP scenarios in cold atoms and molecules [32–38], multilevel atomic and molecular systems, multistate dark-state transport, and related optimized adiabatic-passage protocols [43–49]. More generally, the same strategy should extend beyond state transfer to other multilevel adiabatic-control tasks, including subspace transfer, population routing, shortcut-assisted adiabatic control [55–60], and leakage-suppressed control in superconducting multilevel platforms [62–67]. Related extensions to qudit gate design and synthesis can also be envisaged [76, 77]. We therefore expect this framework to provide a useful starting point for systematically bridging idealized adiabatic-control protocols and realistic multilevel quantum devices.

VI. ACKNOWLEDGEMENT

The research is supported by the National Natural Science Foundation of China (No. 12574082, No. 12174379, No. E31Q02BG), the Chinese Academy of Sciences (No. E0SEBB11, No. E27RBB11), Quantum Science and Technology-National Science and Technology Major Project (No. 2021ZD0302300) and Chinese Academy of Sciences Project for Young Scientists in Basic Research (YSBR-090).

Appendix A: First-Order Optimality Conditions for the Bolza Problem

In this appendix, we derive a practical form of Pontryagin’s maximum principle (PMP) from variational calculus and clarify why the gradient formula used in the main text defines a descent direction. We consider the Bolza functional

$$J[x, u] = \phi(x(T)) + \int_0^T L(x(t), u(t)) dt, \quad (\text{A1})$$

subject to the dynamical constraint

$$c(x, u) \equiv \dot{x}(t) - f(x(t), u(t)) = 0, \quad x(0) = x_0. \quad (\text{A2})$$

Because the dynamics constitute an infinite-dimensional equality constraint in time, it is natural to introduce a time-dependent Lagrange multiplier $\lambda(t)$ and define the augmented Lagrangian

$$\mathcal{L}[x, u, \lambda] = \phi(x(T)) + \int_0^T [L(x, u) + \lambda^T(\dot{x} - f(x, u))] dt. \quad (\text{A3})$$

The first variation with respect to x is

$$\delta_x \mathcal{L} = \phi_x(x(T)) \delta x(T) + \int_0^T [L_x \delta x + \lambda^T (\delta \dot{x} - f_x \delta x)] dt, \quad (\text{A4})$$

where the subscripts denote partial derivatives evaluated along the trajectory $(x(t), u(t))$. Integrating the term containing $\delta \dot{x}$ by parts yields

$$\int_0^T \lambda^T \delta \dot{x} dt = \lambda^T \delta x \Big|_0^T - \int_0^T \dot{\lambda}^T \delta x dt. \quad (\text{A5})$$

Substituting Eq. (A5) into Eq. (A4), we obtain

$$\delta_x \mathcal{L} = [\phi_x(x(T)) + \lambda^T(T)] \delta x(T) - \lambda^T(0) \delta x(0) + \int_0^T (L_x - \lambda^T f_x - \dot{\lambda}^T) \delta x dt. \quad (\text{A6})$$

Because the initial state is fixed, $\delta x(0) = 0$, whereas $\delta x(t)$ is otherwise arbitrary on $(0, T)$. Stationarity therefore yields the costate equation

$$\dot{\lambda}^T(t) = L_x(x(t), u(t)) - \lambda^T(t) f_x(x(t), u(t)), \quad (\text{A7})$$

together with the terminal condition

$$\lambda^T(T) = -\phi_x(x(T)). \quad (\text{A8})$$

We then define the Pontryagin Hamiltonian

$$\mathcal{H}_P(x, u, \lambda) \equiv h(x, u, \lambda) = \lambda^T f(x, u) - L(x, u). \quad (\text{A9})$$

Once Eqs. (A7) and (A8) are imposed, the first variation with respect to the control reduces to

$$\delta \mathcal{L} = \int_0^T (L_u - \lambda^T f_u) \delta u dt = - \int_0^T \frac{\partial h}{\partial u} \delta u dt. \quad (\text{A10})$$

Hence, choosing the control variation as

$$\delta u(t) = \epsilon \frac{\partial h}{\partial u}(x(t), u(t), \lambda(t)), \quad \epsilon > 0, \quad (\text{A11})$$

gives

$$\delta \mathcal{L} = -\epsilon \int_0^T \left\| \frac{\partial h}{\partial u} \right\|^2 dt \leq 0. \quad (\text{A12})$$

Therefore, the PMP gradient defines a local descent direction and drives the objective toward a stationary point of the constrained optimization problem.

Appendix B: Trust-Region Method, Dogleg Strategy, and BFGS Quasi-Newton Update

This appendix summarizes the trust-region framework, the BFGS quasi-Newton curvature update, and the Dogleg strategy used in our numerical optimization [78–81]. Consider the unconstrained problem

$$\min_{x \in \mathbb{R}^n} f(x), \quad (\text{B1})$$

where $f(x)$ is continuously differentiable, and twice differentiable when needed. At the k th iterate x_k , with gradient $g_k = \nabla f(x_k)$, we define the local quadratic model

$$m_k(p) = f(x_k) + g_k^T p + \frac{1}{2} p^T B_k p, \quad (\text{B2})$$

where p is the trial step and B_k is the Hessian or a symmetric approximation to it. The trust-region subproblem is

$$\min_{p \in \mathbb{R}^n} m_k(p) \quad \text{s.t.} \quad \|p\| \leq \Delta_k, \quad (\text{B3})$$

with trust-region radius $\Delta_k > 0$. This constraint reflects the fact that the quadratic model is reliable only within a local neighborhood of x_k .

In practice, constructing the exact Hessian is often expensive, so we update B_k using the BFGS formula. Defining

$$s_k = x_{k+1} - x_k, \quad y_k = g_{k+1} - g_k, \quad (\text{B4})$$

the BFGS update is

$$B_{k+1} = B_k - \frac{B_k s_k s_k^T B_k}{s_k^T B_k s_k} + \frac{y_k y_k^T}{y_k^T s_k}. \quad (\text{B5})$$

This update satisfies the secant condition

$$B_{k+1} s_k = y_k, \quad (\text{B6})$$

and preserves positive definiteness provided that B_0 is symmetric positive definite and the curvature condition

$$y_k^T s_k > 0 \quad (\text{B7})$$

holds. This property is particularly important for the Dogleg method, which relies on a positive-definite quadratic model.

Given a candidate step p_k , the trust-region method compares the actual decrease in f with the decrease predicted by the model:

$$\rho_k = \frac{f(x_k) - f(x_k + p_k)}{m_k(0) - m_k(p_k)}. \quad (\text{B8})$$

A standard radius-update rule is

$$\Delta_{k+1} = \begin{cases} \frac{1}{4} \Delta_k, & \rho_k < \frac{1}{4}, \\ \min(2\Delta_k, \hat{\Delta}), & \rho_k > \frac{3}{4} \text{ and } \|p_k\| = \Delta_k, \\ \Delta_k, & \text{otherwise,} \end{cases} \quad (\text{B9})$$

where $\hat{\Delta}$ is the prescribed maximum radius. The iterate is updated according to

$$x_{k+1} = \begin{cases} x_k + p_k, & \rho_k > \eta, \\ x_k, & \rho_k \leq \eta, \end{cases} \quad (\text{B10})$$

with acceptance threshold $0 < \eta < 1$. In this way, the algorithm suppresses unreliable large steps far from the minimum while recovering fast local convergence near it.

To solve the trust-region subproblem efficiently, we use the Dogleg method. Let

$$p_k^N = -B_k^{-1} g_k \quad (\text{B11})$$

denote the Newton step, which minimizes $m_k(p)$ in the absence of the trust-region constraint. If $\|p_k^N\| \leq \Delta_k$, we simply take

$$p_k = p_k^N. \quad (\text{B12})$$

Along the steepest-descent direction $-g_k$, minimizing the quadratic model yields

$$p_k^U = -\frac{g_k^T g_k}{g_k^T B_k g_k} g_k, \quad (\text{B13})$$

which is the optimal one-dimensional step along $-g_k$. The Dogleg path is then defined by

$$\tilde{p}_k(\tau) = \begin{cases} \tau p_k^U, & 0 \leq \tau \leq 1, \\ p_k^U + (\tau - 1)(p_k^N - p_k^U), & 1 \leq \tau \leq 2. \end{cases} \quad (\text{B14})$$

If $\|p_k^U\| \geq \Delta_k$, the trial step is taken on the boundary along the steepest-descent direction:

$$p_k = -\Delta_k \frac{g_k}{\|g_k\|}. \quad (\text{B15})$$

If $\|p_k^U\| < \Delta_k < \|p_k^N\|$, the accepted step lies on the second segment of the Dogleg path,

$$p_k = p_k^U + \tau_k(p_k^N - p_k^U), \quad 0 < \tau_k < 1, \quad (\text{B16})$$

where τ_k is determined by the boundary condition

$$\|p_k^U + \tau_k(p_k^N - p_k^U)\|^2 = \Delta_k^2. \quad (\text{B17})$$

Defining $d_k = p_k^N - p_k^U$, this is equivalent to the quadratic equation

$$\|d_k\|^2 \tau_k^2 + 2(p_k^U)^T d_k \tau_k + (\|p_k^U\|^2 - \Delta_k^2) = 0, \quad (\text{B18})$$

whose root in $(0, 1)$ gives the required boundary intersection.

In summary, the trust-region framework specifies the local region in which the quadratic model is trusted and provides the step-acceptance criterion, BFGS supplies an efficient curvature approximation, and Dogleg solves the resulting subproblem at low cost while preserving favorable global and local convergence properties.

Appendix C: Circuit Hamiltonian, Sixth-Order Approximation, and Level Spectrum

The Xmon circuit is described by a pair of canonically conjugate operators: the superconducting phase difference $\hat{\phi}$ across the Josephson junction and the Cooper-pair number operator \hat{n} , which satisfy $[\hat{\phi}, \hat{n}] = i$. In the absence of external flux bias, the bare circuit Hamiltonian is

$$H = 4E_C \hat{n}^2 - E_J \cos \hat{\phi}, \quad (\text{C1})$$

where E_C and E_J denote the charging and Josephson energies, respectively. In the transmon regime $E_J \gg E_C$, phase fluctuations are small, so the cosine potential may be expanded about $\hat{\phi} = 0$ up to sixth order:

$$-E_J \cos \hat{\phi} \approx -E_J + \frac{E_J}{2} \hat{\phi}^2 - \frac{E_J}{24} \hat{\phi}^4 + \frac{E_J}{720} \hat{\phi}^6. \quad (\text{C2})$$

Discarding the constant offset $-E_J$, we obtain the effective sixth-order Hamiltonian

$$H^{(6)} = 4E_C \hat{n}^2 + \frac{E_J}{2} \hat{\phi}^2 - \frac{E_J}{24} \hat{\phi}^4 + \frac{E_J}{720} \hat{\phi}^6. \quad (\text{C3})$$

To diagonalize the quadratic part, we introduce bosonic ladder operators a and a^\dagger and define the zero-point fluctuation amplitudes

$$\phi_{\text{zpf}} = \left(\frac{2E_C}{E_J} \right)^{1/4}, \quad n_{\text{zpf}} = \left(\frac{E_J}{32E_C} \right)^{1/4}. \quad (\text{C4})$$

The canonical operators are then written as

$$\hat{\phi} = \phi_{\text{zpf}}(a + a^\dagger), \quad \hat{n} = -i n_{\text{zpf}}(a - a^\dagger). \quad (\text{C5})$$

Substituting these expressions into the quadratic Hamiltonian gives

$$H^{(2)} = 4E_C \hat{n}^2 + \frac{E_J}{2} \hat{\phi}^2 = \hbar\omega_0 \left(a^\dagger a + \frac{1}{2} \right), \quad (\text{C6})$$

with

$$\omega_0 = \frac{\sqrt{8E_J E_C}}{\hbar}. \quad (\text{C7})$$

Including the quartic and sextic terms and retaining the weakly nonlinear contributions within the rotating-wave approximation, the Hamiltonian can be expressed as a polynomial in the number operator. Introducing the small parameter

$$\xi = \sqrt{\frac{2E_C}{E_J}}, \quad (\text{C8})$$

we obtain

$$\hat{H}^{(6)} = \left(\hbar\omega_0 - \frac{E_C}{2} + \frac{E_C \xi}{9} \right) \hat{a}^\dagger \hat{a} + \left(\frac{E_C \xi}{12} - \frac{E_C}{2} \right) (\hat{a}^\dagger \hat{a})^2 + \frac{E_C \xi}{18} (\hat{a}^\dagger \hat{a})^3. \quad (\text{C9})$$

Accordingly, the energy of level $|n\rangle$ within the sixth-order approximation is

$$E_n = \langle n | \hat{H}^{(6)} | n \rangle = \left(\hbar\omega_0 - \frac{E_C}{2} + \frac{E_C \xi}{9} \right) n + \left(\frac{E_C \xi}{12} - \frac{E_C}{2} \right) n^2 + \frac{E_C \xi}{18} n^3, \quad (\text{C10})$$

and the adjacent transition frequencies are

$$\omega_{n+1,n} = \frac{E_{n+1} - E_n}{\hbar}, \quad n = 0, 1, 2, 3. \quad (\text{C11})$$

In the five-level truncation used in this work, the drift Hamiltonian is taken as Eq. (26).

In the eigenbasis $\{|n\rangle\}$, the charge operator in the transmon regime is dominated by nearest-neighbor matrix elements with harmonic-oscillator scaling,

$$\langle j-1 | \hat{n} | j \rangle \approx i n_{\text{zpf}} \sqrt{j}, \quad j = 1, 2, 3, 4. \quad (\text{C12})$$

Hence, within the truncated basis $\{|n\rangle\}_{n=0}^4$,

$$\hat{n} \approx i n_{\text{zpf}} \sum_{j=1}^4 \sqrt{j} \left(|j-1\rangle \langle j| - |j\rangle \langle j-1| \right). \quad (\text{C13})$$

Combining Eq. (C13) with the drive term in Eq. (27) immediately shows that all adjacent transitions are driven simultaneously.

Substituting the two-tone voltage drive of Eq. (28) into the control Hamiltonian and transforming to the interaction picture with respect to H_0 , one obtains

$$H_I(t) = \frac{1}{2} \sum_{j=1}^4 \sqrt{j} \left[\Omega_p(t) e^{i\delta_p^{(j)}(t)} + \Omega_s(t) e^{i\delta_s^{(j)}(t)} \right] |j-1\rangle \langle j| + \text{h.c.}, \quad (\text{C14})$$

where $\Omega_p(t)$ and $\Omega_s(t)$ are the effective Rabi envelopes proportional to $2e n_{\text{zpf}} V_p(t)$ and $2e n_{\text{zpf}} V_s(t)$, respectively. The detuning phases are

$$\delta_p^{(j)}(t) = (\omega_{j,j-1} - \omega_p) t + \phi_p, \quad (\text{C15})$$

$$\delta_s^{(j)}(t) = (\omega_{j,j-1} - \omega_s) t + \phi_s, \quad (\text{C16})$$

with $\omega_{j,j-1} = (E_j - E_{j-1})/\hbar$. This form makes explicit that the same two-tone drive addresses not only the target transitions $|0\rangle \leftrightarrow |1\rangle$ and $|1\rangle \leftrightarrow |2\rangle$, but also off-resonantly drives higher transitions and thereby opens leakage channels.

To obtain an approximately time-independent tridiagonal chain Hamiltonian, we introduce the diagonal unitary transformation

$$U(t) = \sum_{n=0}^4 e^{-i\nu_n t} |n\rangle\langle n|, \quad (\text{C17})$$

with cumulative reference frequencies

$$\nu_0 = 0, \quad \nu_1 = \omega_p, \quad \nu_2 = \omega_p + \omega_s, \quad \nu_3 = 2\omega_p + \omega_s, \quad \nu_4 = 2\omega_p + 2\omega_s. \quad (\text{C18})$$

The rotating-frame Hamiltonian is then

$$H_{\text{rot}}(t) = U^\dagger(t) H(t) U(t) - i\hbar U^\dagger(t) \dot{U}(t), \quad (\text{C19})$$

where $H(t) = H_0 + H_d(t)$. Since $U(t)$ is diagonal, the diagonal terms define the effective detunings

$$\Delta_n = \frac{E_n}{\hbar} - \nu_n, \quad n = 0, 1, 2, 3, 4. \quad (\text{C20})$$

This yields the chain relations

$$\Delta_1 = \omega_{10} - \omega_p, \quad (\text{C21})$$

$$\Delta_2 = \omega_{20} - (\omega_p + \omega_s) = \delta, \quad (\text{C22})$$

$$\Delta_3 = \omega_{30} - (2\omega_p + \omega_s), \quad (\text{C23})$$

$$\Delta_4 = \omega_{40} - (2\omega_p + 2\omega_s). \quad (\text{C24})$$

Under the rotating-wave approximation, one then recovers the five-level chain Hamiltonian of Eq. (29), whose couplings inherit the \sqrt{j} scaling from the charge-operator matrix elements.

-
- [1] S. J. Glaser, U. Boscain, T. Calarco, *et al.*, Training schrödinger's cat: Quantum optimal control: Strategic report on current status, visions and goals for research in europe, *Eur. Phys. J. D* **69**, 279 (2015).
- [2] T. S. Mahesh, P. Batra, and M. H. Ram, Quantum optimal control: Practical aspects and diverse methods, *J. Indian Inst. Sci.* **103**, 591 (2023).
- [3] Q. Ansel, E. Dionis, F. Arrouas, *et al.*, Introduction to theoretical and experimental aspects of quantum optimal control, *J. Phys. B: At. Mol. Opt. Phys.* **57**, 133001 (2024).
- [4] P. de Fouquières, S. G. Schirmer, S. J. Glaser, *et al.*, Second order gradient ascent pulse engineering, *J. Magn. Reson.* **212**, 412 (2011).
- [5] N. Khaneja, T. Reiss, C. Kehlet, *et al.*, Optimal control of coupled spin dynamics: design of NMR pulse sequences by gradient ascent algorithms, *J. Magn. Reson.* **172**, 296 (2005).
- [6] D. M. Reich, M. Ndong, and C. P. Koch, Monotonically convergent optimization in quantum control using krotov's method, *J. Chem. Phys.* **136**, 104103 (2012).
- [7] A. P. Peirce, M. A. Dahleh, and H. Rabitz, Optimal control of quantum-mechanical systems: Existence, numerical approximation, and applications, *Phys. Rev. A* **37**, 4950 (1988).
- [8] J. P. Palao and R. Kosloff, Quantum computing by an optimal control algorithm for unitary transformations, *Phys. Rev. Lett.* **89**, 188301 (2002).
- [9] C. Brif, R. Chakrabarti, and H. Rabitz, Control of quantum phenomena: Past, present, and future, *New J. Phys.* **12**, 075008 (2010).
- [10] D. D'Alessandro, *Introduction to Quantum Control and Dynamics*, 2nd ed. (Chapman and Hall/CRC, New York, 2021).
- [11] D. Sugny and C. Kottz, Optimal control of a three-level quantum system by laser fields plus von neumann measurements, *Phys. Rev. A* **77**, 063420 (2008).
- [12] S. E. Sklarz, D. J. Tannor, and N. Khaneja, Optimal

- control of quantum dissipative dynamics, *Phys. Rev. A* **69**, 053408 (2004).
- [13] M. Werninghaus, D. J. Egger, F. Roy, *et al.*, Leakage reduction in fast superconducting qubit gates via optimal control, *npj Quantum Information* **7**, 14 (2021).
- [14] E. Hyyppä, A. Vepsäläinen, M. Papić, *et al.*, Reducing leakage of single-qubit gates for superconducting quantum processors using analytical control pulse envelopes, *PRX Quantum* **5**, 030353 (2024).
- [15] L. E. Fischer, A. Chiesa, F. Tacchino, *et al.*, Universal qudit gate synthesis for transmons, *PRX Quantum* **4**, 030327 (2023).
- [16] A. Asthana, C. Liu, O. R. Meitei, *et al.*, Leakage reduces device coherence demands for pulse-level molecular simulations, *Phys. Rev. Appl.* **19**, 064071 (2023).
- [17] N. Lacroix, L. Hofele, A. Remm, *et al.*, Fast flux-activated leakage reduction for superconducting quantum circuits, *Phys. Rev. Lett.* **134**, 120601 (2025).
- [18] D. Liberzon, *Calculus of Variations and Optimal Control Theory: A Concise Introduction* (Princeton University Press, Princeton, NJ, 2012).
- [19] U. Boscain, M. Sigalotti, and D. Sugny, Introduction to the pontryagin maximum principle for quantum optimal control, *PRX Quantum* **2**, 030203 (2021).
- [20] A. Garon, S. J. Glaser, and D. Sugny, Time-optimal control of $su(2)$ quantum operations, *Phys. Rev. A* **88**, 043422 (2013).
- [21] V. Evangelakos, E. Paspalakis, and D. Stefanatos, Minimum-time generation of a uniform superposition in a qubit with only transverse field control, *Phys. Rev. A* **108**, 062425 (2023).
- [22] S. Bao, S. Kleer, R. Wang, and A. Rahmani, Optimal control of superconducting qubits using pontryagin's minimum principle: Preparing a maximally entangled state with singular bang-bang protocols, *Phys. Rev. A* **97**, 062343 (2018).
- [23] C. Lin, Y. Wang, G. Kolesov, and U. Kalabić, Application of pontryagin's minimum principle to grover's quantum search problem, *Phys. Rev. A* **100**, 022327 (2019).
- [24] C. Lin, Y. Ma, and D. Sels, Optimal control for quantum metrology via pontryagin's principle, *Phys. Rev. A* **103**, 052607 (2021).
- [25] D. Sugny, C. Kontz, and H. R. Jauslin, Time-optimal control of a two-level dissipative quantum system, *Phys. Rev. A* **76**, 023419 (2007).
- [26] C. Lin, D. Sels, and Y. Wang, Time-optimal control of a dissipative qubit, *Phys. Rev. A* **101**, 022320 (2020).
- [27] H. Jirari, Time-optimal bang-bang control for the driven spin-boson system, *Phys. Rev. A* **102**, 012613 (2020).
- [28] L. V. Lokutsievskiy, A. N. Pechen, and M. I. Zelikin, Time-optimal state transfer for an open qubit, *J. Phys. A: Math. Theor.* **57**, 275302 (2024).
- [29] C. Lin, D. Sels, Y. Ma, and Y. Wang, Stochastic optimal control formalism for an open quantum system, *Phys. Rev. A* **102**, 052605 (2020).
- [30] P. Lewalle and K. B. Whaley, Pontryagin-optimal control of a non-hermitian qubit, *Phys. Rev. A* **107**, 022216 (2023).
- [31] K. Z. Li, J. Z. Tian, and L. T. Xiao, Optimal stimulated raman adiabatic passage using the dynamical quantum geometric tensor, *Phys. Rev. A* **109**, 022443 (2024).
- [32] K. Bergmann, H. Theuer, and B. W. Shore, Coherent population transfer among quantum states of atoms and molecules, *Rev. Mod. Phys.* **70**, 1003 (1998).
- [33] N. V. Vitanov, T. Halfmann, B. W. Shore, *et al.*, Laser-induced population transfer by adiabatic passage techniques, *Annu. Rev. Phys. Chem.* **52**, 763 (2001).
- [34] K. Bergmann, N. V. Vitanov, and B. W. Shore, Perspective: stimulated Raman adiabatic passage: The status after 25 years, *J. Chem. Phys.* **142**, 170901 (2015).
- [35] N. V. Vitanov, A. A. Rangelov, B. W. Shore, *et al.*, Stimulated Raman adiabatic passage in physics, chemistry, and beyond, *Rev. Mod. Phys.* **89**, 015006 (2017).
- [36] J. R. Kuklinski, U. Gaubatz, F. T. Hioe, *et al.*, Adiabatic population transfer in a three-level system driven by delayed laser pulses, *Phys. Rev. A* **40**, 6741 (1989).
- [37] U. Gaubatz, P. Rudecki, S. Schiemann, *et al.*, Population transfer between molecular vibrational levels by stimulated raman scattering with partially overlapping laser fields. a new concept and experimental results, *J. Chem. Phys.* **92**, 5363 (1990).
- [38] P. Král, I. Thanopoulos, and M. Shapiro, Colloquium: Coherently controlled adiabatic passage, *Rev. Mod. Phys.* **79**, 53 (2007).
- [39] T. Kato, On the adiabatic theorem of quantum mechanics, *J. Phys. Soc. Jpn.* **5**, 435 (1950).
- [40] A. Wallraff, D. I. Schuster, A. Blais, *et al.*, Strong coupling of a single photon to a superconducting qubit using circuit quantum electrodynamics, *Nature* **431**, 162 (2004).
- [41] J. Koch, Charge-insensitive qubit design derived from the Cooper pair box, *Phys. Rev. A* **76**, 042319 (2007).
- [42] A. Blais, A. L. Grimsmo, S. M. Girvin, *et al.*, Circuit quantum electrodynamics, *Rev. Mod. Phys.* **93**, 025005 (2021).
- [43] P. J. Pemberton-Ross, A. Kay, and S. G. Schirmer, Quantum control theory for state transformations: Dark states and their enlightenment, *Phys. Rev. A* **82**, 042322 (2010).
- [44] S. Kumar and D. Kumar, Quantum processing by adiabatic transfer through a manifold of dark states, *Phys. Rev. A* **85**, 052317 (2012).
- [45] E. Assémat and D. Sugny, Connection between optimal control theory and adiabatic-passage techniques in quantum systems, *Phys. Rev. A* **86**, 023406 (2012).
- [46] D. Sugny, L. Bomble, T. Ribeyre, *et al.*, Vibrational controlled-not gates using optimized stimulated raman adiabatic passage techniques and optimal control theory, *Phys. Rev. A* **80**, 042325 (2009).
- [47] L. P. Yatsenko, B. W. Shore, and K. Bergmann, Detrimental consequences of small rapid laser fluctuations on stimulated Raman adiabatic passage, *Phys. Rev. A* **89**, 013831 (2014).
- [48] Q. Z. Hou, W. L. Yang, M. Feng, *et al.*, Quantum state transfer using stimulated Raman adiabatic passage under a dissipative environment, *Phys. Rev. A* **88**, 013807 (2013).
- [49] K. Blekos, D. Stefanatos, and E. Paspalakis, Performance of superadiabatic stimulated Raman adiabatic passage in the presence of dissipation and ornstein-uhlenbeck dephasing, *Phys. Rev. A* **102**, 023715 (2020).
- [50] A. Vezvaei, E. Takou, P. Hilaire, and others, Avoiding leakage and errors caused by unwanted transitions in lambda systems, *PRX Quantum* **4**, 030312 (2023).
- [51] F. Motzoi, J. M. Gambetta, P. Rebentrost, and F. K. Wilhelm, Simple pulses for elimination of leakage in weakly nonlinear qubits, *Phys. Rev. Lett.* **103**, 110501 (2009).
- [52] J. M. Gambetta, F. Motzoi, S. T. Merkel, *et al.*, Analytic

- control methods for high-fidelity unitary operations in a weakly nonlinear oscillator, *Phys. Rev. A* **83**, 012308 (2011).
- [53] M. Demirplak and S. A. Rice, On the consistency, extremal, and global properties of counterdiabatic fields, *J. Chem. Phys.* **129**, 154111 (2008).
- [54] M. V. Berry, Transitionless quantum driving, *J. Phys. A: Math. Theor.* **42**, 365303 (2009).
- [55] D. Guéry-Odelin, A. Ruschhaupt, A. Kiely, E. Torrontegui, *et al.*, Shortcuts to adiabaticity: Concepts, methods, and applications, *Rev. Mod. Phys.* **91**, 045001 (2019).
- [56] Y.-C. Li and X. Chen, Shortcut to adiabatic population transfer in quantum three-level systems: effective two-level problems and feasible counterdiabatic driving, *Phys. Rev. A* **94**, 063411 (2016).
- [57] Y.-X. Du, Z.-T. Liang, Y.-C. Li, *et al.*, Experimental realization of stimulated Raman shortcut-to-adiabatic passage with cold atoms, *Nat. Commun.* **7**, 12479 (2016).
- [58] V. Evangelakos, E. Paspalakis, and D. Stefanatos, Optimal STIRAP shortcuts using the spin-to-spring mapping, *Phys. Rev. A* **107**, 052606 (2023).
- [59] A. Baksic, H. Ribeiro, and A. A. Clerk, Speeding up adiabatic quantum state transfer by using dressed states, *Phys. Rev. Lett.* **116**, 230503 (2016).
- [60] I. Čepaitė, A. Polkovnikov, A. J. Daley, *et al.*, Counterdiabatic optimized local driving, *PRX Quantum* **4**, 010312 (2023).
- [61] X. Zhao, L.-M. Kuang, and J.-Q. Liao, General dark-state theory for arbitrary multilevel quantum systems, *Phys. Rev. A* **113**, 013723 (2026).
- [62] K. Kumar, A. Vepsäläinen, S. Danilin, *et al.*, Stimulated Raman adiabatic passage in a three-level superconducting circuit, *Nat. Commun.* **7**, 10628 (2016).
- [63] H. Xu, C. Song, W. Liu, *et al.*, Coherent population transfer between uncoupled or weakly coupled states in ladder-type superconducting qutrits, *Nat. Commun.* **7**, 11018 (2016).
- [64] A. Vepsäläinen, S. Danilin, and G. S. Paraoanu, Superadiabatic population transfer in a three-level superconducting circuit, *Sci. Adv.* **5**, eaau5999 (2019).
- [65] W. Zheng, Y. Zhang, Y. Dong, *et al.*, Optimal control of stimulated raman adiabatic passage in a superconducting qudit, *npj Quantum Information* **8**, 9 (2022).
- [66] J. Niu, B.-J. Liu, Y. Zhou, *et al.*, Customizable quantum control via stimulated raman user-defined passage, *Phys. Rev. Appl.* **17**, 034056 (2022).
- [67] U. Singhal, H. V. Upadhyay, I. Ahmad, *et al.*, Robust gates inspired by stimulated raman adiabatic passage for a superconducting dual-rail qubit, *Phys. Rev. Appl.* **23**, 014044 (2025).
- [68] H.-S. Chang, Y. P. Zhong, A. Bienfait, *et al.*, Remote entanglement via adiabatic passage using a tunably dissipative quantum communication system, *Phys. Rev. Lett.* **124**, 240502 (2020).
- [69] F. Petziol, B. Dive, S. Carretta, *et al.*, Accelerating adiabatic protocols for entangling two qubits in circuit QED, *Phys. Rev. A* **99**, 042315 (2019).
- [70] M. M. Mahana, S. Davuluri, and T. N. Dey, Coherent population transfer with polariton states in circuit QED, *Phys. Rev. A* **110**, 023716 (2024).
- [71] L. S. Pontryagin, V. G. Boltyanskii, R. V. Gamkrelidze, *et al.*, *The Mathematical Theory of Optimal Processes* (Interscience Publishers, New York, 1962).
- [72] J. R. Johansson, P. D. Nation, and F. Nori, QuTiP: An open-source python framework for the dynamics of open quantum systems, *Comput. Phys. Commun.* **183**, 1760 (2012).
- [73] N. Lambert, E. Giguère, P. Menczel, *et al.*, Qutip 5: The quantum toolbox in python, *Phys. Rep.* **1153**, 1 (2026).
- [74] V. V. Sivak, A. Eickbusch, H. Liu, *et al.*, Model-free quantum control with reinforcement learning, *Phys. Rev. X* **12**, 011059 (2022).
- [75] B. Sarma and M. J. Hartmann, Designing fast quantum gates using optimal control with a reinforcement-learning ansatz, *Phys. Rev. Appl.* **23**, 014015 (2025).
- [76] S. Omanakuttan, A. Mitra, E. J. Meier, *et al.*, Qudit entanglers using quantum optimal control, *PRX Quantum* **4**, 040333 (2023).
- [77] L. M. Seifert, Z. Li, T. Roy, *et al.*, Exploring ququart computation on a transmon using optimal control, *Phys. Rev. A* **108**, 062609 (2023).
- [78] M. J. D. Powell, A hybrid method for nonlinear equations, in *Numerical Methods for Nonlinear Algebraic Equations*, edited by P. Rabinowitz (Gordon and Breach, New York, 1970).
- [79] R. Fletcher, A new approach to variable metric algorithms, *The Computer Journal* **13**, 317 (1970).
- [80] J. J. Moré and D. C. Sorensen, Computing a trust region step, *SIAM Journal on Scientific and Statistical Computing* **4**, 553 (1983).
- [81] Y.-X. Yuan, Recent advances in trust region algorithms, *Math. Program.* **151**, 249 (2015).